ELSEVIER

International Journal of Heat and Fluid Flow 23 (2002) 471–486

International Journal of HEAT AND FLUID FLOW

www.elsevier.com/locate/ijhff

Evaporation of acoustically levitated droplets of binary liquid mixtures

Alexander L. Yarin [a,*], Günter Brenn [b,*,1], Dirk Rensink [b]

[a] *Faculty of Mechanical Engineering, Technion—Israel Institute of Technology, Haifa 32000, Israel*
[b] *Lehrstuhl für Strömungsmechanik, University of Erlangen–Nürnberg, Cauerstraße 4, 91058 Erlangen, Germany*

Received 25 April 2001; accepted 1 February 2002

Abstract

The present work deals with the evaporation of acoustically levitated droplets. It was shown before by the authors that droplets of pure liquids in acoustic levitators evaporate mostly due to the convective effect of the acoustic streaming arising near the free droplet surface. In the present work acoustically levitated droplets of binary liquid mixtures are considered. The theoretical model of acoustically driven droplet evaporation, as developed in an earlier publication of the authors, is extended for these liquids, and experimental investigations on the evaporation of droplets consisting of the liquids are conducted. Results from theory and experiment are compared and discussed.

Keywords: Acoustic levitation; Drop evaporation; Binary mixtures; Aqueous solutions; Theoretical mass transfer model

1. Introduction

Drying processes of droplets in a gas are of significant importance for many applications. Diffusion and ordinary convection-driven evaporation of multicomponent drops of miscible liquids were investigated theoretically and experimentally in a number of previous studies, e.g. (Law and Binark, 1979; Law et al., 1987; Annamalai et al., 1993; Renksizbulut and Bussmann, 1993; Chen et al., 1997). These show that the evaporation rate of solution droplets during their lifetime is variable, which results in a nonlinear dependence $d^2(t)$, where d is the volume-equivalent droplet diameter and t is time.

The drying of droplets of liquid mixtures and solids solutions is of significant interest in many industrial applications, where, e.g., the liquid vapor is a fuel for combustion processes or powders are produced by spray drying processes. Several works exist on this topic, but no archival publication is known where an acoustic levitator was used to acquire experimental data about the d^2 dependency on time. Note, however, some preliminary attempts in the thesis (Daidzic, 1995). Unfortunately, these results cannot be used even for comparison, since they lack most of the needed details.

In a recent study on droplets of pure liquids evaporating in acoustic levitators with strong acoustic fields it was shown that the acoustic streaming in the gas provides a convective mechanism much stronger than the ordinary one and dominates the evaporation in this case (Yarin et al., 1999).

The aim of the present work is to investigate theoretically and experimentally the evaporation of solution droplets levitated in strong acoustic fields. Binary mixtures of miscible liquids are considered. The process of evaporation of single droplets is first theoretically analyzed, and the theory is then verified using experimental data acquired with an acoustic levitator. In Section 2 some physical estimates for the evaporation process are presented. The model of the acoustically driven evaporation of miscible liquids is described in Section 3. The solution of the model equations is discussed in Section 4. In Section 5 the force balance in the acoustic droplet levitation is discussed. The experimental setup is described in Section 6. Section 7 discusses the comparison

* Corresponding authors. Tel.: +972-4-8293473; fax: +972-4-8324533.

E-mail addresses: meralya@yarin.technion.ac.il (A.L. Yarin), brenn@lstm.uni-erlangen.de (G. Brenn).

[1] Tel.: +49-9131-8529501; fax: +49-9131-8529503.

0142-727X/02/$ - see front matter
PII: S0142-727X(02)00142-X

Nomenclature

a	volume-equivalent radius of the droplet (m)
A	coefficient in Eq. (33)
A_{0e}	effective pressure amplitude in the incident acoustic wave at $t = 0$ (kg/m s^2)
B_0, B	initial and current gas particle velocity amplitude in the sound wave (m/s)
c_{sb}	vapor concentration at the droplet surface (kg/m^3); subscript s means the steady part (cf. Yarin et al., 1999)
$c_{s\infty}$	vapor concentration at the outer boundary of the acoustic boundary layer (kg/m^3)
c_0	sound velocity (m/s)
d	volume-equivalent droplet diameter (m)
D	binary diffusion coefficient in liquid/liquid systems (m^2/s)
D_0	diffusion coefficient of vapor in air (m^2/s)
E	coefficient in Eq. (33)
F	group given by Eq. (40)
g	gravity acceleration (m/s^2)
G	dimensionless group given by (21)
$\langle\overline{h}_c\rangle$	time-averaged mass transfer coefficient in the acoustically driven evaporation, averaged over the droplet surface (m/s)
$\langle\overline{h}_T\rangle$	heat transfer coefficient (kg/s^{3}K)
I_v	latent heat of evaporation (m^2/s^2)
k_a	thermal conductivity of air (kg m/s^{3}K)
K	dimensionless coefficient of mass transfer
K_i	coefficients given by Eq. (43a)–(43c) (kg/kmol)
L_{dw}, L_{wd}	factors in the expressions for the activity coefficients
L_*	characteristic scale of the toroidal vortices (m)
M	molecular mass (kg/kmol)
N	group introduced in Eq. (36) (m^3/kg)
$p_{1,sat}$	saturation vapor pressure (kg/m s^2)
P_i	coefficients given by Eq. (48a)–(48c) (kg/kmol)
r	radial coordinate (m)
R	absolute gas constant (J/K mol)
s_l, s_s	lengths of the major and minor semiaxes of the meridional contour of the droplet (m)
t, t_1	time (s)
T	temperature (K)
T_s	temperature of the droplet surface (K)
V_0	initial droplet volume (m^3)
$\dot{V}$	volumetric rate of air blowing (m^3/s)
Y	mass fraction
$\overline{Y}$	average mass fraction
Y_c	dimensionless group given by Eq. (22b)
Z, Z_w, Z_d	mole fractions

Greeks

α	thermal diffusivity of liquid (m^2/s)
$\gamma, \gamma_w, \gamma_d$	activity coefficient
κ_0	thermal diffusivity of air (m^2/s)
λ_0	sound wavelength (m)
ν	kinematic viscosity (m^2/s)
ξ	spacial dimensionless coordinate associated with the moving free surface
ρ	liquid density (kg/m^3)
ρ_0	unperturbed gas density (kg/m^3)
$\overline{\rho_\ell}$	average density of the mixture (kg/m^3)
σ	surface tension coefficient (kg/s^2)
$\overline{\sigma_\ell}$	surface tension coefficient of the mixture (kg/s^2)
τ_1	characteristic heat transfer time (s)
τ_2	characteristic diffusion time (s)
τ_3	droplet lifetime (s)
τ_B	characteristic "blowing" time (s)
τ_{Di}	characteristic time of the diffusion losses of vapor from the toroidal vortices (s)
$\overline{\tau}$	replaces $\overline{t}$ as per Eq. (26)
ω	angular frequency of the incident sound wave (s^{-1})

Subscripts

0	properties related to $t = 0$
1	properties related to the solvent
2	properties related to the solute
a	properties related to $r = a$

of the theoretical and experimental results. Conclusions from the present work are drawn in Section 8.

2. Physical estimates

The evaporation of a multicomponent droplet in stagnant, convective, or acoustic environment inevitably results in heat transfer and diffusion of components inside the droplet. As a characteristic droplet size we take the droplet volume-equivalent radius $a \sim 10^{-3}$ m. The thermal diffusivity α of such liquids as water and methanol is of the order of $\alpha \sim 10^{-7}$ m^2/s. Therefore the characteristic heat transfer time for such droplets is of the order

$$\tau_1 = \frac{a^2}{\alpha} \sim 10 \text{ s}. \tag{1}$$

On the other hand, the binary diffusion coefficient D in liquid/liquid systems is of the order of $D \sim 10^{-9}$ m^2/s (Kays (1975) on p. 374 gives $\nu/D \sim 10^3$, which yields for the kinematic viscosity of $\nu \sim 10^{-6}$ m^2/s the above-

mentioned order of magnitude of D). Therefore the characteristic diffusion time inside the droplet is of the order

$$\tau_2 = \frac{a^2}{D} = 10^3 \text{ s}. \tag{2}$$

Given the fact that the lifetime of an acoustically levitated droplet evaporating due to the acoustic streaming is of the order of $\tau_3 \sim 10^2$ to 10^3 s, we can conclude that $\tau_1 \ll \tau_3$, whereas $\tau_2 \sim \tau_3$. Therefore the lumped-capacity description can be applied in the analysis of the droplet temperature, which is also supported by the estimate of the Biot number. Therefore a reasonable approximation is that there is a uniform temperature distribution $T \equiv T_s$ (T_s is the temperature of the droplet surface) inside the droplet which is found from the lumped-capacity thermal balance. On the other hand, due to the fact that $\tau_2 \sim \tau_3$, the species concentrations inside the droplet during its acoustically driven evaporation cannot be assumed uniform. They must be calculated using a pointwise solution of the diffusion equations inside the droplet.

3. Diffusion of species inside droplets of binary liquid/liquid mixtures and problem formulation for the acoustically driven evaporation

In the present section we consider the evaporation of a droplet of two miscible volatile liquids, where the two components evaporate simultaneously from the droplet surface. Y_1 and Z_1 are used to denote the mass and mole fractions of the liquid, which we call the solvent, and Y_2 and Z_2 for the second component of the mixture, which we call the solute. The relations between these parameters are given by the following expressions:

$$Y_1 = \frac{Z_1 M_1}{Z_1 M_1 + Z_2 M_2}, \tag{3a}$$

$$Y_2 = \frac{Z_2 M_2}{Z_1 M_1 + Z_2 M_2}, \tag{3b}$$

$$Z_1 = \frac{Y_1 M_2}{Y_1 M_2 + (1 - Y_1) M_1}, \tag{3c}$$

$$Z_2 = \frac{(1 - Y_1) M_1}{Y_1 M_2 + (1 - Y_1) M_1}, \tag{3d}$$

where M_1 and M_2 are the molecular masses of the solvent and solute, respectively. Obviously, $0 \leqslant Y_i \leqslant 1$, $0 \leqslant Z_i \leqslant 1$, and $Y_1 + Y_2 = 1$, and $Z_1 + Z_2 = 1$.

We consider now the diffusion equation for the solvent inside the droplet assuming for simplicity spherical symmetry with $a(t)$ being the volume-equivalent droplet radius corresponding to a real droplet squeezed to some extent by the acoustic field (Yarin et al., 1998). The equation has the form

$$\frac{\partial Y_1}{\partial t} = \frac{D}{r^2} \frac{\partial}{\partial r} \left(r^2 \frac{\partial Y_1}{\partial r} \right), \tag{4}$$

where r is the radial coordinate. Eq. (4) is supplemented by the following boundary conditions

$$\frac{\partial Y_1}{\partial r} = 0 \quad \text{at the droplet center } r = 0 \text{ and } t > 0, \tag{5a}$$

$$-\rho_1 D \frac{\partial Y_1}{\partial r} - \frac{\mathrm{d}a}{\mathrm{d}t} \rho_1 Y_1 = \overline{\langle h_{c1} \rangle} (c_{sb1} - c_{s\infty 1})$$
$$\text{at the droplet surface } r = a(t) \text{ and } t > 0. \tag{5b}$$

The boundary condition (5b) expresses the fact that the solvent losses from the droplet result from a purely diffusional mass flux as well as from the propagation of the evaporation front (the free surface) towards the droplet center. The corresponding two terms stand on the left in (5b). On the other hand, the solvent vapor leaving the droplet is propelled outwards by the mass flux sustained by the acoustic streaming in the gas near the droplet surface. This acoustically driven mass flux stands on the right-hand side in (5b), where $\overline{\langle h_{c1} \rangle}$ is the time-averaged mass transfer coefficient also averaged over the droplet surface, which is denoted by the overbar. The symbols c_{sb1} and $c_{s\infty 1}$ denote the solvent vapor concentration at the droplet surface and at the outer boundary of the acoustic boundary layer (in the large toroidal acoustically driven outer vortices), respectively. A description of the toroidal vortices can be found in Yarin et al. (1999). The mass transfer coefficient $\overline{\langle h_{c1} \rangle}$ has been calculated in Yarin et al. (1999) and is given by the expressions (9.1)–(9.4) and (6.34) there. Also the vapor concentration at the outer boundary of the acoustic boundary layer has been calculated in Yarin et al. (1999). In the present context it will be discussed below.

For a pure liquid

$$(c_{sb1})_{\text{pure solvent}} = \frac{p_{1,\text{sat}}(T_s) M_1}{R T_s}, \tag{6}$$

where $p_{1,\text{sat}}$ is the saturation vapor pressure at the droplet surface temperature T_s, given by the Antoine equation, and R is the absolute gas constant.

In the case of a dilute solution, Raoult's law is valid, and thus (Klotz and Rosenberg, 1994)

$$(c_{sb1})_{\text{dilute solution}} = Z_1 (c_{sb1})_{\text{pure solvent}}. \tag{7}$$

To extend the Raoult's law to the range of non-dilute solutions, the activity coefficient γ_1 is introduced (Klotz and Rosenberg, 1994; Hirata et al., 1975), which yields

$$c_{sb1} = \gamma_1 Z_1 \frac{p_{1,\text{sat}}(T_s) M_1}{R T_s}. \tag{8}$$

Expression (8) should be substituted into the boundary condition (5b) which takes the following form

$$-\rho_1 D \frac{\partial Y_1}{\partial r} - \frac{\mathrm{d}a}{\mathrm{d}t} \rho_1 Y_1 = \overline{\langle h_{c1} \rangle} \left[\gamma_1 Z_1 \frac{p_{1,\text{sat}}(T_s) M_1}{R T_s} - c_{s\infty 1} \right] \tag{9}$$

at the droplet surface $r = a(t)$.

The activity coefficient $\gamma_1 = \gamma_w$ is given in Hirata et al. (1975). In our notation it reads

$$\gamma_w = \frac{1}{Z_w + L_{wd}Z_d}\exp\left[-Z_d\left(\frac{L_{dw}}{Z_d + L_{dw}Z_w} - \frac{L_{wd}}{L_{wd}Z_d + Z_w}\right)\right], \tag{10}$$

where $Z_w = Z_1$, $Z_d = 1 - Z_1$, and the coefficients L_{dw} and L_{wd} characteristic of a specific liquid pair are also given in the above reference. For example, for water/methanol mixtures $L_{dw} = 0.418$ and $L_{wd} = 0.9699$, and for water/ethanol mixtures $L_{dw} = 0.1108$ and $L_{wd} = 0.956$.

The problem at hand is an initial value problem. We know, however, practically nothing about the initial distribution of the components inside the droplet. Therefore, we assume an initial average value of the mass fraction of the solvent in the droplet $\overline{Y}_1$

$$t = 0 \quad \overline{Y}_1 = Y_{10} = \frac{Z_{10}M_1}{Z_{10}M_1 + Z_{20}M_2}, \tag{11}$$

where the initial mole fraction of solvent Z_{10} is given.

Expression (11) is used as an initial condition for Eq. (4).

Similarly, the distribution of solute inside the droplet is described by the following problem

$$\frac{\partial Y_2}{\partial t} = \frac{D}{r^2}\frac{\partial}{\partial r}\left(r^2\frac{\partial Y_2}{\partial r}\right), \tag{12a}$$

$$\frac{\partial Y_2}{\partial r} = 0 \quad \text{at } r = 0 \text{ and } t > 0, \tag{12b}$$

$$-\rho_1 D\frac{\partial Y_2}{\partial r} - \frac{da}{dt}\rho_1 Y_2 = \langle\overline{h_{c2}}\rangle\left[\gamma_2 Z_2\frac{p_{2,sat}(T_s)M_2}{RT_s} - c_{s\infty 2}\right] \quad \text{at } r = a(t) \text{ and } t > 0, \tag{12c}$$

$$\overline{Y}_2 = Y_{20} = \frac{Z_{20}M_2}{Z_{10}M_1 + Z_{20}M_2} \quad t = 0, \tag{12d}$$

where the activity coefficient $\gamma_2 = \gamma_d$ is given in Hirata et al. (1975). In the present notation it reads

$$\gamma_d = \frac{1}{Z_d + L_{dw}Z_w}\exp\left[Z_w\left(\frac{L_{dw}}{Z_d + L_{dw}Z_w} - \frac{L_{wd}}{L_{wd}Z_d + Z_w}\right)\right], \tag{13}$$

The mass transfer coefficient $\langle\overline{h_{c2}}\rangle$ is calculated as in Yarin et al. (1999). The concentration of the solute vapor outside the acoustic boundary layer $c_{s\infty 2}$, similar to the solvent vapor there, is also calculated as in Yarin et al. (1999). Some details on $c_{s\infty 1}$ and $c_{s\infty 2}$ will be discussed below.

Adding (9) and (12c) and using the fact that $Y_1 + Y_2 = 1$, we obtain the equation describing the evolution of the droplet radius during the acoustically driven evaporation

$$\rho_1\frac{da}{dt} = -\left\{\langle\overline{h_{cl}}\rangle\left[\frac{p_{1,sat}(T_s)M_1}{RT_s}\gamma_1 Z_{1a} - c_{s\infty 1}\right] + \langle\overline{h_{c2}}\rangle\left[\frac{p_{2,sat}(T_s)M_2}{RT_s}\gamma_2 Z_{2a} - c_{s\infty 2}\right]\right\} \tag{14}$$

which is identical to the overall mass balance for the droplet. In Eq. (14) $Z_{1a} = Z_1(r = a)$ and $Z_{2a} = Z_2(r = a)$.

To be able to calculate Z_{1a} and Z_{2a}, the diffusion problems inside the droplet must be solved to find the mass (or mole) fraction distributions along the droplet radius at each instant of time. To do that, it is convenient to introduce a new spatial coordinate ξ associated with the moving free surface of the droplet

$$t_1 = t, \tag{15a}$$

$$\xi = \frac{r}{a(t)}. \tag{15b}$$

In the new variables, Eqs. (4) and (12a) take the form

$$a^2\frac{\partial Y_i}{\partial t} - \xi a\frac{da}{dt}\frac{\partial Y_i}{\partial \xi} = \frac{D}{\xi^2}\frac{\partial}{\partial \xi}\left(\xi^2\frac{\partial Y_i}{\partial \xi}\right), \tag{16}$$

where $i = 1, 2$ and subscript 1 is dropped in the new time variable.

We render the equations dimensionless by the following scales—the initial volume-equivalent droplet radius a_0 for a, and the time scale $\rho_1 a_0^{3/2}/\{[c_{sbl}(T_{s0}) - c_{s\infty 10}]\sqrt{B_0 D_{01}}\}$ for t, where T_{s0} is the initial droplet temperature, D_{01} the diffusion coefficient of the solvent vapor in air, $c_{s\infty 10}$ the solvent vapor concentration in the toroidal vortices at $t = 0$,

$$c_{sb1}(T_{s0}) = \frac{p_{1,sat}(T_{s0})M_1}{RT_{s0}} \tag{17}$$

and the gas particle velocity amplitude in the sound wave

$$B_0 = \frac{A_{0e}(t = 0)}{\rho_0 c_0}. \tag{18}$$

The effective pressure amplitude of the incident acoustic field at $t = 0$ is denoted $A_{0e}(t = 0)$, ρ_0 is the unperturbed gas density, and c_0 is the sound velocity.

Using the mass transfer coefficients $\langle\overline{h_{c1}}\rangle$ and $\langle\overline{h_{c2}}\rangle$ calculated using (9.1)–(9.3) and (6.34) of Yarin et al. (1999), we obtain from (5a), (9), (11), (12a)–(12d), (13), (14), (15a), (15b) and (16) the following dimensionless equations of the problem:

$$\frac{d\overline{a}^2}{d\overline{t}} = -K\sqrt{\frac{A_{0e}(\overline{t})/\rho_0 c_0^2}{\omega a_0/c_0}}\sqrt{\frac{\overline{B}}{B_0}}\left\{\left(\left[c_{sb1}Z_1(1,\overline{t})\gamma_1 - c_{s\infty 1}\right] + \sqrt{D_{02}/D_{01}}\left[c_{sb2}Z_2(1,\overline{t})\gamma_2 - c_{s\infty 2}\right]\right)/[c_{sb1}(T_{s0}) - c_{s\infty 10}]\right\}, \tag{19a}$$

$$Z_1(1,\overline{t}) = \frac{Y_1|_{\xi=1}M_2}{Y_1|_{\xi=1}M_2 + (1 - Y_1|_{\xi=1})M_1}, \tag{19b}$$

$$Z_2(1,\bar{t}) = 1 - Z_1(1,\bar{t}), \tag{19c}$$

and

$$\overline{a}^2 \frac{\partial Y_1}{\partial \bar{t}} = G \frac{1}{\xi^2} \frac{\partial}{\partial \xi}\left(\xi^2 \frac{\partial Y_1}{\partial \xi}\right) + \frac{\xi}{2} \frac{\mathrm{d}\overline{a}^2}{\mathrm{d}\bar{t}} \frac{\partial Y_1}{\partial \xi}, \tag{20a}$$

$$\xi = 0: \quad \frac{\partial Y_1}{\partial \xi} = 0 \text{ at } \bar{t} > 0, \tag{20b}$$

$$\xi = 1: \quad -2\frac{\partial Y_1}{\partial \xi} - \frac{1}{G} Y_1 \frac{\mathrm{d}\overline{a}^2}{\mathrm{d}\bar{t}} = \frac{D_{01}}{D} K \frac{B}{\sqrt{\omega D_{01}}} \frac{\left[c_{\mathrm{sb1}} Z_1(1,\bar{t})\gamma_1 - c_{\mathrm{s}\infty 1}\right]}{\rho_1} \text{ at } \bar{t} > 0, \tag{20c}$$

$$\bar{t} = 0: \quad \overline{Y}_1 = Y_{10}, \tag{20d}$$

where the dimensionless group G is given by

$$G = \frac{\rho_1 \sqrt{D/D_{01}}}{[c_{\mathrm{sb1}}(T_{\mathrm{s}0}) - c_{\mathrm{s}\infty 10}]} \sqrt{\frac{D}{B_0 a_0}}. \tag{21}$$

The following notation is used in (19a)–(19c), (20a)–(20d): K is the coefficient of mass transfer due to the acoustically driven evaporation defined by (9.1)–(9.4) in Yarin et al. (1999), ω is the angular frequency of the incident sound wave (corresponding to the ultrasonic range), D_{02} is the solute vapor diffusion coefficient in air, D is the binary diffusion coefficient in the solution, and overbars denote the dimensionless variables.

Note also that the vapor concentrations outside the outer boundary of the acoustic boundary layer are calculated using the approach of Yarin et al. (1999), which results in the following expressions:

$$c_{\mathrm{s}\infty i} = \gamma_i Z_i(1,\bar{t}) \times \frac{Y_{\mathrm{c}}}{Y_{\mathrm{c}} + (\tau_{\mathrm{B}}^{-1} + \tau_{\mathrm{D}i}^{-1}) c_{\mathrm{sb1}}(T_{\mathrm{s}0})/[\rho_1 \sqrt{D_{0\mathrm{i}}/D_{01}}]}, \tag{22a}$$

$$Y_{\mathrm{c}} = 2\pi \left(\frac{a_0}{L_*}\right)^3 \left(\overline{a}^2\right)^{1/2} K \sqrt{\frac{A_{0\mathrm{e}}(\bar{t})/\rho_0 c_0^2}{\omega a_0/c_0}} \sqrt{\frac{B}{B_0}}, \tag{22b}$$

where $i = 1,\ 2$ and L_* is the characteristic scale of the toroidal vortices, and according to Yarin et al. (1999)

$$\tau_{\mathrm{B}}^{-1} = \frac{\rho_1 \dot{V}}{a_0^{3/2}[c_{\mathrm{sb1}}(T_{\mathrm{s}0}) - c_{\mathrm{s}\infty 10}]\sqrt{B_0 D_{01}}} \left(\frac{a_0}{L_*}\right)^3, \tag{23a}$$

$$\tau_{\mathrm{D}i}^{-1} = \frac{\rho_1 D_{0\mathrm{i}}}{a_0^{1/2}} \frac{(4\pi)^{2/3} 3^{1/3}}{[c_{\mathrm{sb1}}(T_{\mathrm{s}0}) - c_{\mathrm{s}\infty 10}]\sqrt{B_0 D_{01}}} \left(\frac{a_0}{L_*}\right)^2. \tag{23b}$$

In the expression for the characteristic "blowing" time τ_{B}, $\dot{\mathbf{V}}$ is the rate of blowing; $\tau_{\mathrm{D}i}$ $(i = 1, 2)$ are the characteristic "diffusion" times for the diffusion losses of the solvent and solute vapor from the toroidal vortices. In this context "blowing" means a ventilation air stream applied experimentally to deplete liquid vapor from the toroidal vortices in order to prevent its accumulation there. The accumulation of vapor would lead to an unsteady vapor concentration in the ambient of the droplet.

The droplet temperature is found from the lumped-capacity thermal balance for the droplet

$$\langle \overline{h}_{\mathrm{T}} \rangle (T_\infty - T_{\mathrm{s}}) = \langle \overline{h_{\mathrm{c}1}} \rangle \left[\frac{p_{1,\mathrm{sat}}(T_{\mathrm{s}}) M_1}{R T_{\mathrm{s}}} I_{\mathrm{v}1} Z_1(1,\bar{t}) \gamma_1\right] + \langle \overline{h_{\mathrm{c}2}} \rangle \left[\frac{p_{2,\mathrm{sat}}(T_{\mathrm{s}}) M_2}{R T_{\mathrm{s}}} I_{\mathrm{v}2} Z_2(1,\bar{t}) \gamma_2\right], \tag{24}$$

where $\langle \overline{h_{\mathrm{T}}} \rangle$ is the heat transfer coefficient, T_∞ is the gas temperature at infinity, and $I_{\mathrm{v}i}$ are the latent heat of evaporation of the solvent $(i = 1)$ and solute $(i = 2)$. Note that in (24) we neglect the thermal effect of vapor condensation back on the droplet.

Similarly to Yarin et al. (1999) we rearrange Eq. (24) to the following equation for T_{s}:

$$T_{\mathrm{s}} = \mathrm{Y} + \left\{ \mathrm{Y}^2 - \frac{D_{01}}{k_{\mathrm{a}}} \left(\frac{\kappa_0}{D_{01}}\right)^{1/2} \left[\frac{p_{1,\mathrm{sat}}(T_{\mathrm{s}}) M_1}{R} I_{\mathrm{v}1} Z_1(1,\bar{t}) \gamma_1\right] - \frac{1}{k_{\mathrm{a}}} (D_{02}\kappa_0)^{1/2} \left[\frac{p_{2,\mathrm{sat}}(T_{\mathrm{s}}) M_2}{R} I_{\mathrm{v}2} Z_2(1,\bar{t}) \gamma_2\right] \right\}^{1/2} \tag{25a}$$

$$Y = \frac{1}{2}\left[T_\infty + \left(\frac{\kappa_0}{D_{01}}\right)^{1/2} \frac{D_{01} M_1 \mathrm{I}_{v1}}{k_{\mathrm{a}} R} \frac{p_\infty H}{T_\infty}\right], \tag{25b}$$

where k_{a} and κ_0 are the thermal conductivity and diffusivity of air. This equation is solved iteratively at each time step, since in distinction from Yarin et al. (1999), Eq. (25a) and (25b) incorporates the mole fractions $Z_1(1,\bar{t})$ and $Z_2(1,\bar{t})$ which are time dependent.

It is emphasized that, in the case of the acoustically driven evaporation of the levitated mixture droplets of the present work, Eqs. (19a), (22a), (22b), (23a), (23b) and (25a), (25b) replace (9.5a), (9.6), (9.5d,e) and (8.11) of Yarin et al. (1999). As in the latter work, Eq. (19a) is solved numerically. In the present case, however, the mole fractions $Z_1(1,\bar{t})$ and $Z_2(1,\bar{t})$ should be determined by solving in parallel the problem ((20a)–(20d)). The next section is devoted to the solution of this problem.

4. Solution of the diffusion problem

To solve the diffusion problem we shall use an integral method reminiscent of the Karman–Pohlhausen integral method used in the boundary layer theory (Schlichting, 1979). It will allow us to reduce the solution of the diffusion problem to an ordinary differential equation instead of the partial one. Denoting

$$\overline{\tau} = \int_0^{\bar{t}} \frac{\mathrm{d}\bar{t}}{\overline{a}^2(\bar{t})} \tag{26}$$

we rewrite Eq. (20a) as

$$\frac{\partial Y_1\xi^2}{\partial\overline{\tau}} = G\frac{\partial}{\partial\xi}\left(\xi^2\frac{\partial Y_1}{\partial\xi}\right) + \frac{\xi^3}{2}\frac{\mathrm{d}\overline{a}^2}{\mathrm{d}\overline{t}}\frac{\partial Y_1}{\partial\xi} \tag{27}$$

and integrate it over ξ:

$$\frac{\mathrm{d}}{\mathrm{d}\overline{\tau}}\int_0^1 Y_1\xi^2\,\mathrm{d}\xi = G\xi^2\frac{\partial Y_1}{\partial\xi}\bigg|_0^1 + \frac{1}{2}\frac{\mathrm{d}\overline{a}^2}{\mathrm{d}\overline{t}}\int_0^1 \xi^3\frac{\partial Y_1}{\partial\xi}\,\mathrm{d}\xi. \tag{28}$$

Taking the last integral by parts and introducing $\overline{t}$, we reduce Eq. (28) to the following one:

$$\frac{\mathrm{d}}{\mathrm{d}\overline{t}}\left[\overline{\mathrm{a}}^3\int_0^1 \xi^2 Y_1\,\mathrm{d}\xi\right] = \frac{\overline{a}}{2}\left[2G\frac{\partial Y_1}{\partial\xi}\bigg|_{\xi=1} + \frac{\mathrm{d}\overline{a}^2}{\mathrm{d}\overline{t}}Y_1\bigg|_{\xi=1}\right]. \tag{29}$$

The physical meaning of this equation is elucidated if it is written in a rearranged form. To do that we note that the boundary condition (20c) using (21) takes the form:

$$2G\frac{\partial Y_1}{\partial\xi}\bigg|_{\xi=1} + \frac{\mathrm{d}\overline{a}^2}{\mathrm{d}\overline{t}}Y_1\bigg|_{\xi=1} = -\frac{B}{\sqrt{\omega B_0 a_0}}K\frac{[c_{\mathrm{sb1}}Z_1(1,\overline{t})\gamma_1 - c_{\mathrm{s}\infty1}]}{c_{\mathrm{sb1}}(T_{\mathrm{s}0}) - c_{\mathrm{s}\infty10}}. \tag{30}$$

Substituting (30) into (29) and making use of the fact that (Yarin et al., 1999)

$$\frac{\langle\overline{h_{\mathrm{c1}}}\rangle 2a}{D_{01}} = K\frac{B}{\sqrt{\omega D_{01}}} \tag{31}$$

we can rearrange Eq. (29) to the following dimensional form

$$\rho_1\frac{\mathrm{d}}{\mathrm{d}t}\left[4\pi\int_0^a r^2 Y_1\,\mathrm{d}r\right] = -4\pi a^2\langle\overline{h_{\mathrm{c1}}}\rangle[c_{\mathrm{sb1}}Z_1(1,\mathrm{t})\gamma_1 - c_{\mathrm{s}\infty1}] \tag{32}$$

which manifests itself the overall mass balance of the solvent in the droplet. Therefore the dimensionless Eq. (29) expresses the overall mass balance of the solvent in the droplet.

We assume the following distribution of the mass fraction of solvent in the droplet

$$Y_1 = A(\overline{t})\xi^2 + E(\overline{t}), \tag{33}$$

where the boundary condition at $\xi = 0$ (20b) is satisfied automatically and the coefficients $A(\overline{t})$ and $E(\overline{t})$ may be found as functions of time satisfying with the help of (33) the integral Eq. (29) and the boundary condition (30).

The accuracy of the assumption (33) in the framework of the integral method can be estimated only in comparison with the results of an exact analytical or a numerical solution. The latter are not available, however, for the present problem. In the framework of the boundary layer theory, a kindred Karman–Pohlhausen integral method was extensively tested against the analytical and numerical results in Chapter X in Schlichting (1979). The comparisons show that the integral method is, in general, rather accurate, which allows us to believe in its accuracy also in the present case.

Substituting (33) into (29), we obtain

$$\frac{\mathrm{d}}{\mathrm{d}\overline{t}}\left[\frac{\overline{a}^3}{3}(A+E) - \overline{a}^3\frac{2}{15}A\right] = \frac{\overline{a}}{2}\left[4G\cdot A + \frac{\mathrm{d}\overline{a}^2}{\mathrm{d}\overline{t}}(A+E)\right]. \tag{34}$$

On the other hand, from (30) we obtain

$$4G\cdot A + (A+E)\frac{\mathrm{d}\overline{a}^2}{\mathrm{d}\overline{t}} = -\frac{B}{\sqrt{\omega B_0 a_0}}K\frac{1}{c_{\mathrm{sb1}}(T_{\mathrm{s}0}) - c_{\mathrm{s}\infty10}} \times\left[c_{\mathrm{sb1}}\gamma_1\frac{(A+E)M_2}{(A+E)(M_2-M_1)+M_1} - c_{\mathrm{s}\infty1}\right]. \tag{35}$$

Denoting

$$N = \frac{B}{\sqrt{\omega B_0 a_0}}K\frac{1}{c_{\mathrm{sb1}}(T_{\mathrm{s}0}) - c_{\mathrm{s}\infty10}} \tag{36}$$

and accounting for the fact that

$$Y_1(1,\overline{t}) = A + E \tag{37}$$

we obtain from (35) the following

$$A = -\frac{Y_1(1,\overline{t})}{4G}\frac{\mathrm{d}\overline{a}^2}{\mathrm{d}\overline{t}} - \frac{N}{4G}\left[c_{\mathrm{sb1}}\gamma_1\frac{Y_1(1,\overline{t})M_2}{Y_1(1,\overline{t})(M_2-M_1)+M_1} - c_{\mathrm{s}\infty1}\right]. \tag{38}$$

Note that the coefficient A characterizing the solvent mass flux in the liquid phase at the droplet surface may be positive since $\mathrm{d}\overline{a}^2/\mathrm{d}\overline{t} < 0$. In this case the solvent mass fraction at the droplet surface is higher than in the center, whereas the solute concentration at the surface is lower due to its fast evaporation. For smaller D the value of A is larger and the concentration field in the droplet is less uniform. When the liquid solute evaporates totally, A approaches zero and the solvent concentration field becomes uniform. For small $|\mathrm{d}\overline{a}^2/\mathrm{d}t|$ the coefficient A may be negative.

Also we obtain from (34)

$$\frac{\mathrm{d}F}{\mathrm{d}\overline{t}} = -\frac{\overline{a}}{2}N\left[c_{\mathrm{sb1}}\gamma_1\frac{Y_1(1,\overline{t})M_2}{Y_1(1,\overline{t})(M_2-M_1)+M_1} - c_{\mathrm{s}\infty1}\right], \tag{39}$$

where

$$F = \frac{\overline{a}^3}{3}Y_1(1,\overline{t}) + \overline{a}^3\frac{2}{15}\left\{\frac{Y_1(1,\overline{t})}{4G}\frac{\mathrm{d}\overline{a}^2}{\mathrm{d}\overline{t}} + \frac{N}{4G}\left[c_{\mathrm{sb1}}\gamma_1\frac{Y_1(1,\overline{t})M_2}{Y_1(1,\overline{t})(M_2-M_1)+M_1} - c_{s\infty1}\right]\right\} \tag{40}$$

Eq. (39) is integrated numerically together with Eq. (19a) to find $F(\overline{t})$.Then at each time step $Y_1(1,\overline{t})$ is found from (40). Noting that Eq. (19a) may be rewritten as

$$\frac{\mathrm{d}\overline{a}^2}{\mathrm{d}\bar{t}} = -N\left\{\left[c_{\mathrm{sb1}}Z_1(1,\bar{t})\gamma_1 - c_{\mathrm{s}\infty 1}\right] + \sqrt{\frac{D_{02}}{D_{01}}}\left[c_{\mathrm{sb2}}(1-Z_1(1,\bar{t}))\gamma_2 - c_{\mathrm{s}\infty 2}\right]\right\} \tag{41}$$

and substituting the latter into (40), we obtain the following expression for $Y_1(1,\bar{t})$:

$$Y_1(1,\bar{\mathrm{t}}) = -\frac{K_2}{2K_1} + \sqrt{\frac{K_2^2}{4K_1^2} - \frac{K_3}{K_1}} \tag{42}$$

The coefficients K_i in (42) are given by the following formulae:

$$K_1 = \frac{\overline{a}^3}{3}(M_2 - M_1) + \overline{a}^3\frac{2}{15}\left[-\frac{N}{4G}\left\{c_{\mathrm{sb1}}\gamma_1 M_2 - c_{\mathrm{s}\infty 1}(M_2 - M_1) + \sqrt{\frac{D_{02}}{D_{01}}}[-c_{\mathrm{sb2}}\gamma_2 M_1 - c_{\mathrm{s}\infty 2}(M_2 - M_1)]\right\}\right], \tag{43a}$$

$$K_2 = -F(M_2 - M_1) + \frac{\overline{a}^3}{3}M_1 + \overline{a}^3\frac{2}{15}\left[-\frac{N}{4G}\left\{-c_{\mathrm{s}\infty 1}M_1 + \sqrt{\frac{D_{02}}{D_{01}}}[c_{\mathrm{sb2}}\gamma_2 M_1 - c_{\mathrm{s}\infty 2}M_1]\right\} + \frac{N}{4G}\{c_{\mathrm{sbl}}\gamma_1 M_2 - c_{\mathrm{s}\infty 1}(M_2 - M_1)\}\right], \tag{43b}$$

$$K_3 = -M_1 F + \overline{a}^3\frac{2}{15}\left[-\frac{N}{4G}c_{\mathrm{s}\infty 1}M_1\right]. \tag{43c}$$

The average value of the mass fraction of solvent in the drop $\overline{Y}_1$ is given by

$$\overline{Y}_1 = \int_0^a Y_1 4\pi r^2\,\mathrm{d}r\left(\frac{4}{3}\pi a^3\right)^{-1}. \tag{44}$$

Rendering it dimensionless, we obtain

$$\overline{Y}_1 = 3\int_0^1 Y_1\xi^2\,\mathrm{d}\xi. \tag{45}$$

Substituting (33) into (45) and accounting for (37), we obtain

$$\overline{Y}_1 = Y_1(1,\bar{t}) - \frac{2}{5}A. \tag{46}$$

According to Eq. (20d) we impose the initial condition $\bar{t} = 0$, $\overline{Y}_1 = Y_{10}$. Then substituting (38) and (41) into (46), we solve it to find the mass fraction of the solvent at the droplet surface at the initial instant $Y_1(1,0)$:

$$Y_1(1,0) = -\frac{P_2}{2P_1} + \sqrt{\frac{P_2^2}{4P_1^2} - \frac{P_3}{P_1}}. \tag{47}$$

The coefficients P_i in (47) are given by the following formulae:

$$P_1 = (M_2 - M_1) + \frac{2}{5}\left[-\frac{N}{4G}\left\{c_{\mathrm{sb1}}\gamma_1 M_2 - c_{\mathrm{s}\infty 1}(M_2 - M_1) + \sqrt{\frac{D_{02}}{D_{01}}}[-c_{\mathrm{sb2}}\gamma_2 M_1 - c_{\mathrm{s}\infty 2}(M_2 - M_1)]\right\}\right], \tag{48a}$$

$$P_2 = -Y_{10}(M_2 - M_1) + M_1 + \frac{2}{5}\left[-\frac{N}{4G}\left\{-c_{\mathrm{s}\infty 1}M_1 + \sqrt{\frac{D_{02}}{D_{01}}}[c_{\mathrm{sb2}}\gamma_2 M_1 - c_{\mathrm{s}\infty 2}M_1]\right\} + \frac{N}{4G}[c_{\mathrm{sb1}}\gamma_1 M_2 - c_{\mathrm{s}\infty 1}(M_2 - M_1)]\right], \tag{48b}$$

$$P_3 = -M_1 Y_{10} + \frac{2}{5}\left[-\frac{N}{4G}c_{\mathrm{s}\infty 1}M_1\right], \tag{48c}$$

Expressions (47) and (48a)–(48c) allow us to find $Y_1(1,0)$. Using this we find the value of F at $\bar{t} = 0$ from (40), which is used as an initial condition for the integration of (39).

5. Force balance in the levitation of solution droplets

To calculate the weight of an acoustically levitated solution droplet, we need to find its average density $\overline{\rho_\ell}$ at each instant of time. Assuming that the solution is ideal (and thus it does not change volume when pure components are mixed), we obtain the rule of Amagat

$$\overline{\rho_\ell} = \frac{1}{\overline{Y}_1/\rho_1 + (1-\overline{Y}_1)/\rho_2}, \tag{49}$$

where the average mass fraction of solvent $\overline{Y}_1$ is found from (46) and (38), and ρ_2 is the pure solute density.

To calculate the levitation force one needs to find an instantaneous droplet shape (Yarin et al., 1998, 1999), which involves an instantaneous value of the surface tension as a function of $Y_1(1,\bar{t})$. Similarly to (49) we take the following approximation for the surface tension of mixtures

$$\overline{\sigma}_l = \frac{1}{Y_1(1,\bar{\mathrm{t}})/\sigma_1 + [1 - Y_1(1,\bar{\mathrm{t}})]/\sigma_2}, \tag{50}$$

where σ_1 and σ_2 are the surface tension coefficients of the pure solvent and solute.

Expression (50) has been checked against the experimental data published in Wohlfarth and Wohlfarth (1997). The comparison presented in Fig. 1 shows that the proposed approximation is very accurate for water/methanol mixtures, and less accurate (with an offset of about 25%) for water/ethanol mixtures.

The droplet weight is equilibrated by the acoustic levitation force. The equilibrium is described in Yarin et al. (1998). Using (49) and (50), the calculation of the droplet equilibrium position is performed along the same lines in the present work.

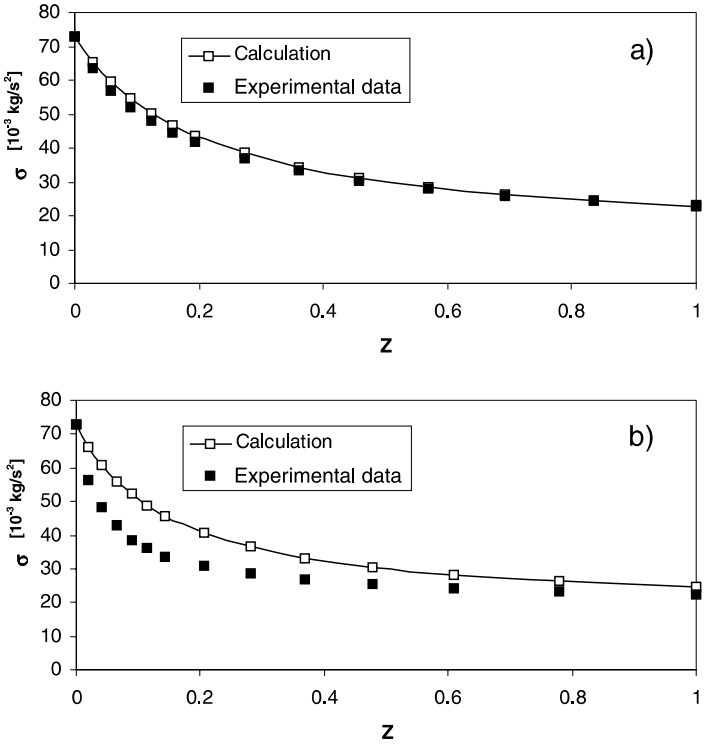

Fig. 1. Surface tension of binary water/methanol and water/ethanol mixtures. The curves with open symbols show the results calculated using Eq. (50), the filled symbols—the data from Wohlfarth and Wohlfarth (1997) for (a) water/methanol and (b) water/ethanol. The symbols Z denote the mole fractions of the alcohols.

6. Experimental set-up and technique

The theoretical work of the present paper is accompanied by experimental investigations on the evaporation of droplets of binary liquid mixtures. For these experiments, the ultrasonic levitator together with an image analysis system already used by the authors in Yarin et al. (1999) was employed for determining the droplet shape and therefore the droplet volume as a function of time. The whole experimental apparatus is sketched in Fig. 2. The ultrasonic levitator supplied by Battelle Frankfurt (Germany) is characterised by the vibration frequency of the ultrasound transducer of 56 kHz. This frequency corresponds to the nominal sound wavelength $\lambda_0 = 0.61 \times 10^{-2}$ m at an unperturbed air temperature $T_0 = 293$ K, when the unperturbed sound velocity in air $c_0 = 343.8$ m/s. It was shown in Yarin et al. (1998) that the harmonic content of the acoustic field in the levitator may be approximated safely by a single standing harmonic wave. The ultrasound waves are reflected from the concave surface of a round reflector plate positioned opposite to the transducer at a

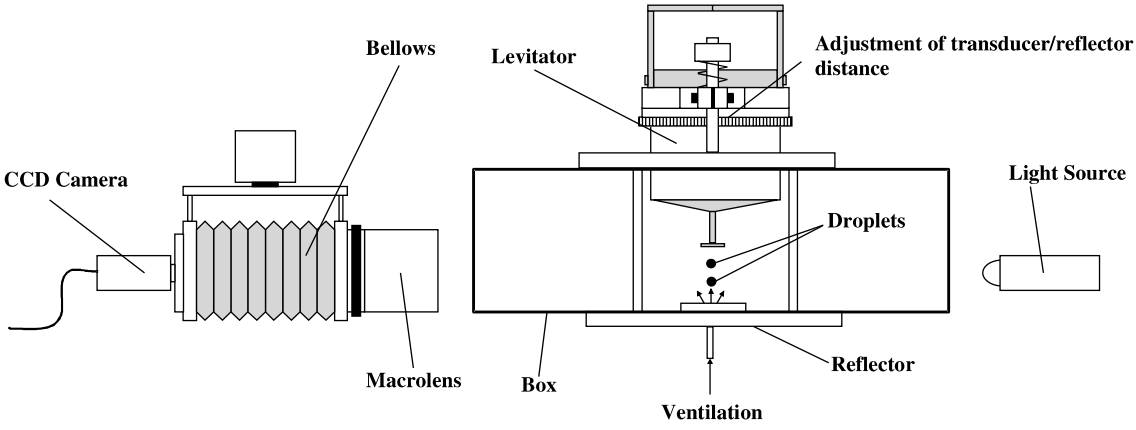

Fig. 2. Sketch of the experimental set-up.

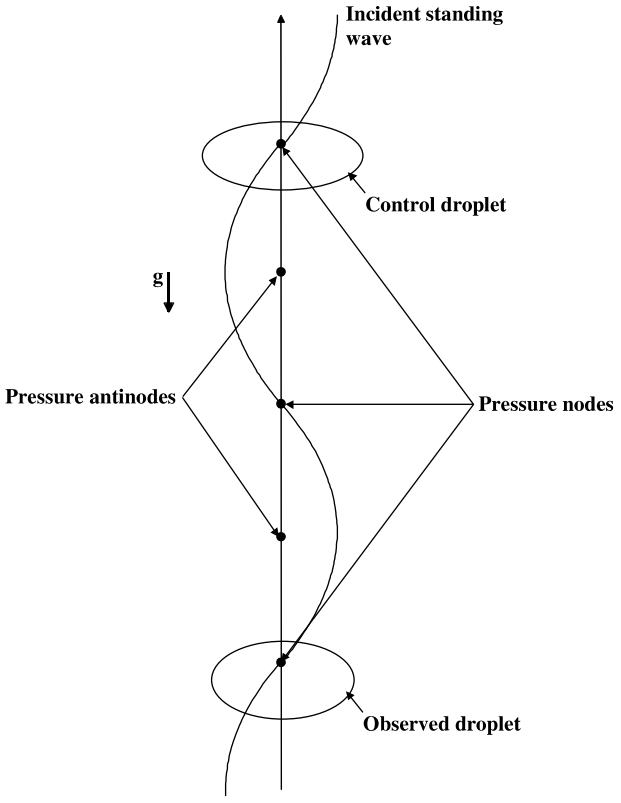

Fig. 3. Sketch of the relative droplet positions in the acoustic field.

distance of 2.86×10^{-2} m, which is appropriate to allow for the formation of eight pressure nodes in this resonator. The distance between the transducer and the reflector can be adjusted with an uncertainty of the order of 20 μm. The relative positions of the transducer and reflector were kept constant throughout the measurements, and no active control of the sound pressure level (SPL) was applied.

A hole with a diameter of 9 mm was drilled in the centre of the reflector. Through this hole an air stream with a relative humidity (water content) of <2% was blown out towards the droplet to ventilate the droplet environment. This is necessary to prevent an enrichment of liquid vapour in the droplet vicinity due to trapping of the vapour in the vortices driven by the acoustic waves (acoustic streaming). The details of this technique were discussed in Yarin et al. (1999).

The droplets to be investigated are produced using a microliter syringe. For producing the drop, the liquid is sucked into the syringe, and the volume of liquid representing the initial drop volume is pressed out of the syringe needle after it has been put close to the ultrasonic resonator. The drop is then inserted into the ultrasonic field, where the SPL has to be raised strongly to overcome the adhesion force which attaches the drop to the needle. After the subsequent adjustment of the appropriate SPL at which the experiment is to be started, the drop is ready for the measurements. The SPL is determined from the aspect ratio of the drop shape for a given liquid and a given drop volume.

For determining the droplet shape as a function of time, an imaging system is used. The particular parts of the system are a CCD video camera with macrolens and a PC equipped with a frame-grabber card and the software OPTIMAS. For imaging, the drop is illuminated from behind using a white light source. The drop is imaged using a large magnification factor, which is determined before the measurement series by imaging a

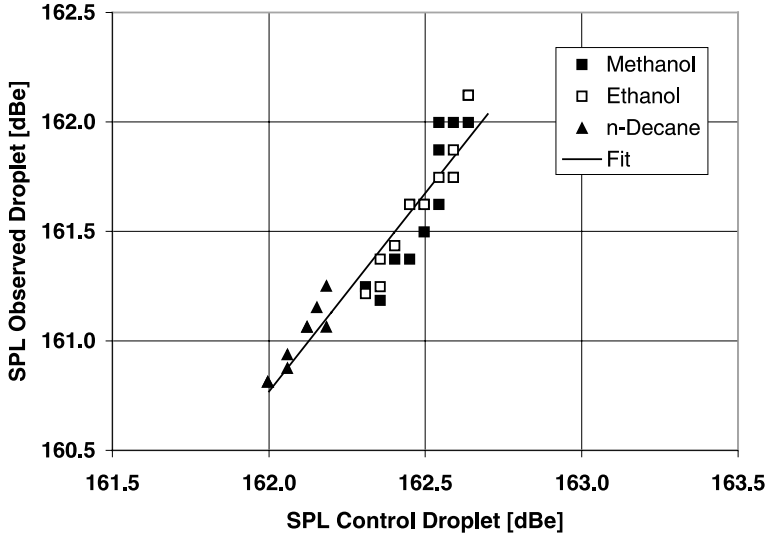

Fig. 4. Result of the calibration measurements with pure methanol, ethanol and *n*-decane as the observed droplets and *n*-hexadecane as the control one. The data are shown together with a linear fit ($R_* = 0.95$). Different points for the same liquid in the observed droplet actually correspond to different moments of time. The SPL increases as the observed droplet evaporates.

high-precision microscale etched on a glass plate. Based on this high-quality image of the drop, the image analysis software provides detailed information on the visible meridional section of the drop.

6.1. Sound pressure level calibration

The ultrasonic field, characterised by the SPL, greatly influences the heat and mass transfer between the droplet and the ambient air. Therefore it is important to know the value of the SPL and its change in the course of evaporation. In Yarin et al. (1999) it was shown that the SPL increases with decreasing droplet volume, since the influence of scattering at the droplet surface decreases. For pure liquids it is enough to measure volume and aspect ratio of the droplet as functions of time to determine the SPL, which can then be used for numerical calculations since the droplet shape is a result of force equilibrium between surface tension and the acoustic pressure acting on the droplet surface. However, for mixtures the surface tension changes with the liquid composition, so that at least the mass fraction of one component must be known to calculate the SPL. Since this is very difficult, another method is used to determine the SPL. If a second droplet (hereinafter called the "control droplet") consisting of a pure, non-volatile liquid is levitated together with the evaporating liquid mixture droplet, this droplet can be used as a probe to measure the SPL for the evaporating droplet (hereinafter called the "observed droplet"). A sketch of the relative droplet positions is depicted in Fig. 3. Both droplets have a combined influence on the acoustic field. This interaction is only dependent on the droplet volumina and the aspect ratios of the spheroidal droplet shapes, but not directly on the droplet composition.

To determine the relation between the SPL felt by the control and the observed droplets, calibration measurements have first been performed. In these calibration measurements, the observed droplet consisted of a pure liquid to determine the SPL from its volume and aspect ratio. As liquids of the observed droplet methanol, ethanol and *n*-decane were used. The control

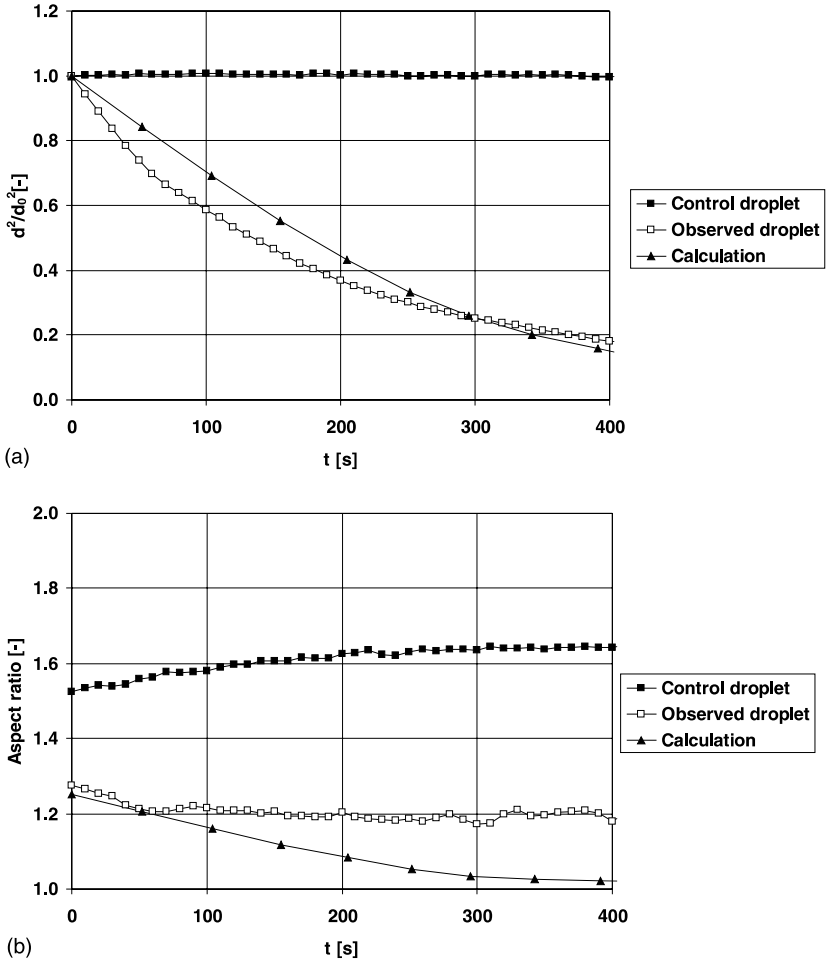

Fig. 5. Experimental and computational results for water/methanol droplets with an initial water mass fraction of 25%: (a) normalized droplet surface and (b) aspect ratios of control and observed droplets. The initial volume of the droplets was 2.54 μl.

droplet consisted of *n*-hexadecane in all cases, a non-volatile liquid which was previously well investigated in acoustic levitators (e.g. Yarin et al., 1998). Since the interaction between the droplets depends on their volume, it is important to point out that the volume of the control droplet was kept constant for all measurements presented here. The control droplet volume was chosen to be 2.4 μl. The control droplet was positioned above the observed droplet with one node spacing, as sketched in Fig. 3. The ventilating effect of the jet was not disturbed. Since the acoustic transducer was located on the top of the resonator, the observed droplet was located in the acoustic wake of the control droplet. This reduces the SPL felt by the observed droplet as compared to the control droplet, which is supported by the data discussed in the following paragraph.

During the calibration measurements, the observed droplet evaporates and the volume and aspect ratios of both droplets were recorded simultaneously as functions of time. After finishing these measurements the SPLs for both droplets were calculated using the theory described in Yarin et al. (1999), since first the observed droplets were pure liquids like the control one. The result is shown in Fig. 4. A linear fit of the form $\mathrm{SPL}_{\mathrm{obs}} = A_* + B_* \mathrm{SPL}_{\mathrm{cont}}$ reveals a correlation with a coefficient of $R_* = 0.95$, where the parameters $A_* = -132.53$ and $B_* = 1.81$. The results for different liquids in the observed droplet collapse on a single line.

In the experiments with mixtures, the control droplet was still pure *n*-hexadecane. It has been used to record the SPL at its location. Then the above correlation was used to find the SPL experienced by the observed droplet.

6.2. Uncertainty analysis

Before starting a measurement, a droplet with known (initial) volume is inserted into the ultrasonic field. For doing this, a desired volume of the liquid in the microliter syringe is pressed out of the syringe needle. This volume may be chosen with an uncertainty of ± 0.05 μl. This error level is given by the scale and the properties of the syringe.

Furthermore, the measurement of the equivalent drop size from the meridional contour of the levitated droplet is based on its visualization. The contour is

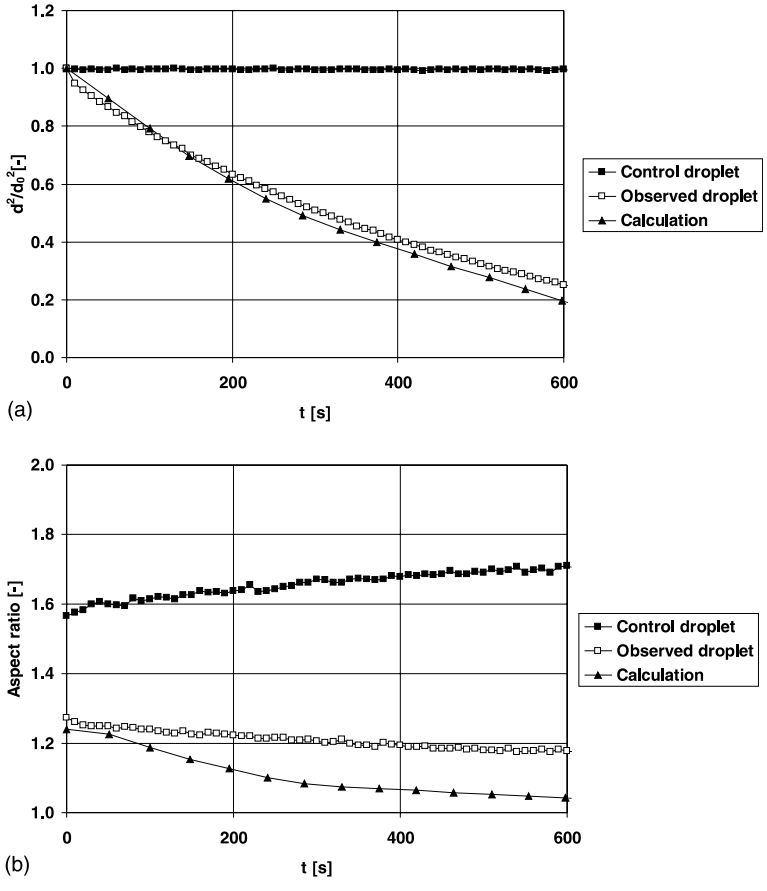

Fig. 6. Experimental and computational results for water/methanol droplets with an initial water mass fraction of 50%: (a) normalized droplet surface and (b) aspect ratios of control and observed droplets. The initial volume of the droplets was 3.86 μl.

Table 1
Initial and ambient conditions in the experiments with binary liquid mixture droplets

Mixture	Initial mass fraction water (%)	Initial drop volume (μl)	Ambient temperature (°C)
Water/Methanol	25	2.54	25
Water/Methanol	50	3.86	25
Water/Methanol	75	2.18	25
Water/Ethanol	25	2.69	24
Water/Ethanol	50	2.51	24
Water/Ethanol	75	3.76	24

approximated by an ellipse. The related data then consist of the coordinates of points of the imaged droplet contour, the lengths of the major and minor semiaxes s_l and s_s and the aspect ratio s_l/s_s of the fitted oblate ellipse which approximates the drop shape. If the droplet image is ideally sharp, the accuracy of the approximation of the drop contour by the ellipse is better than 2% in the representation of the major and minor semiaxes. The calculation of the volume-equivalent drop diameter then is carried out accurately based on the equation

$$d = 2\sqrt[3]{s_l^2 s_s}. \tag{51}$$

6.3. Measurements

Measurements on the evaporation of liquid mixture droplets were carried out using water/methanol and water/ethanol mixtures with initial water mass fractions of 25%, 50% and 75%. The initial and ambient conditions for the experiments are listed in Table 1.

Since the stability of two droplets being levitated at the same time in the acoustic field differs from what is known from single droplet levitation, an operation window concerning tuning (distance between transducer and reflector) and levitator driving voltage had first to be found. In single droplet levitation it is sufficient to set

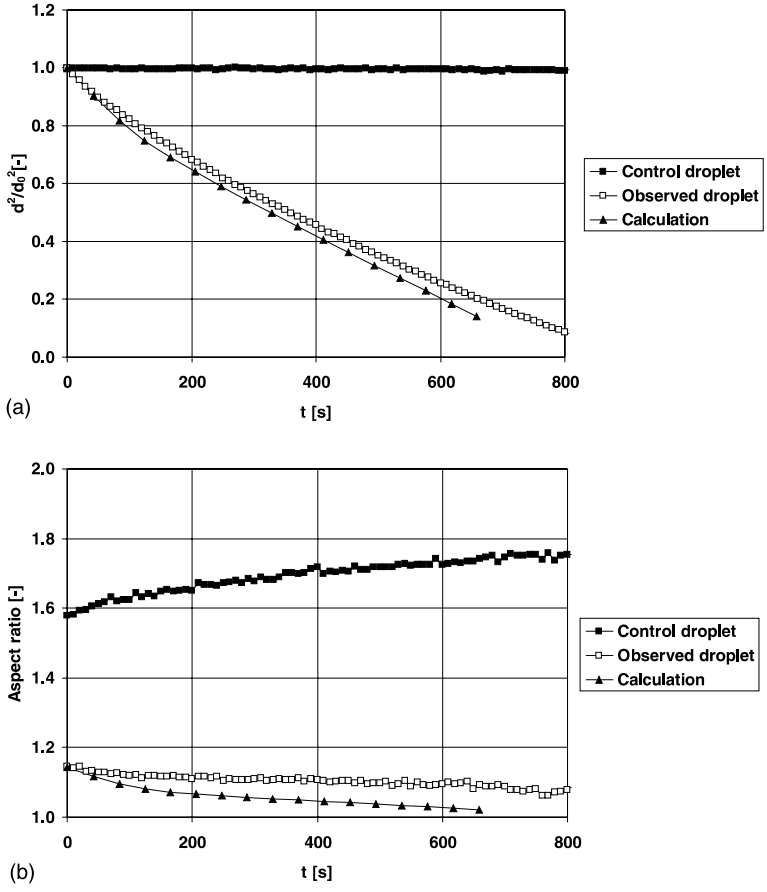

Fig. 7. Experimental and computational results for water/methanol droplets with an initial water mass fraction of 75%: (a) normalized droplet surface and (b) aspect ratios of control and observed droplets. The initial volume of the droplets was 2.18 μl.

the distance of transducer and reflector close to a multiple of the half wavelength of the acoustic wave and then adjust the driving voltage to obtain a sufficient levitation force. In the case of two droplets, however, the observed droplet causes an aerodynamic wake from the ventilating air stream. This wake affects the control drop located above (i.e. downstream from) the observed drop, causing radial oscillations of the control drop. This drop motion increases the uncertainty of measurements of its aspect ratio and, therefore, contributes to the fluctuations of the data points in Fig. 4. It turned out that this effect could be minimized by adjusting the distance between the transducer and reflector, so that radial motions of the control droplet only occurred at small volumes of the observed droplet of approx. 0.1 μl, i.e. at the late stages of the evaporation.

7. Discussion of the results

To compare the experimental results with the calculations, the droplet surface, normalized with its initial value, and the aspect ratio were considered as functions of time. The results for water/methanol mixtures are depicted in Figs. 5–7, and for water/ethanol mixtures in Figs. 8–10. The subfigures (a) represent the normalized droplet surface, and (b) the aspect ratio.

A comparison of the experimental results with the calculations for the liquid mixtures reveals a good agreement for the normalised surface as a function of time for mixtures with an initial water mass fraction of 50% and 75% (subfigures (a) in Figs. 6, 7, 9 and 10). The initial aspect ratio exhibits good agreement between measurement and calculation for water/methanol mixtures, as depicted in subfigures (b) of Figs. 5–7, but a significant deviation for water/ethanol mixtures (subfigures (b) in Figs. 8–10). The deviation in the aspect ratio increases for all mixtures with ongoing time.

The comparison of the calculations with the experimental data shows that the mass transfer from the droplet for mixtures with an initial water mass fraction of 50% and more is described correctly. The poor representation of the aspect ratio in the calculations indicates that the calculation of the mixture surface tension must be improved. The latter can also be responsible for the deviations of the results with an initial water mass

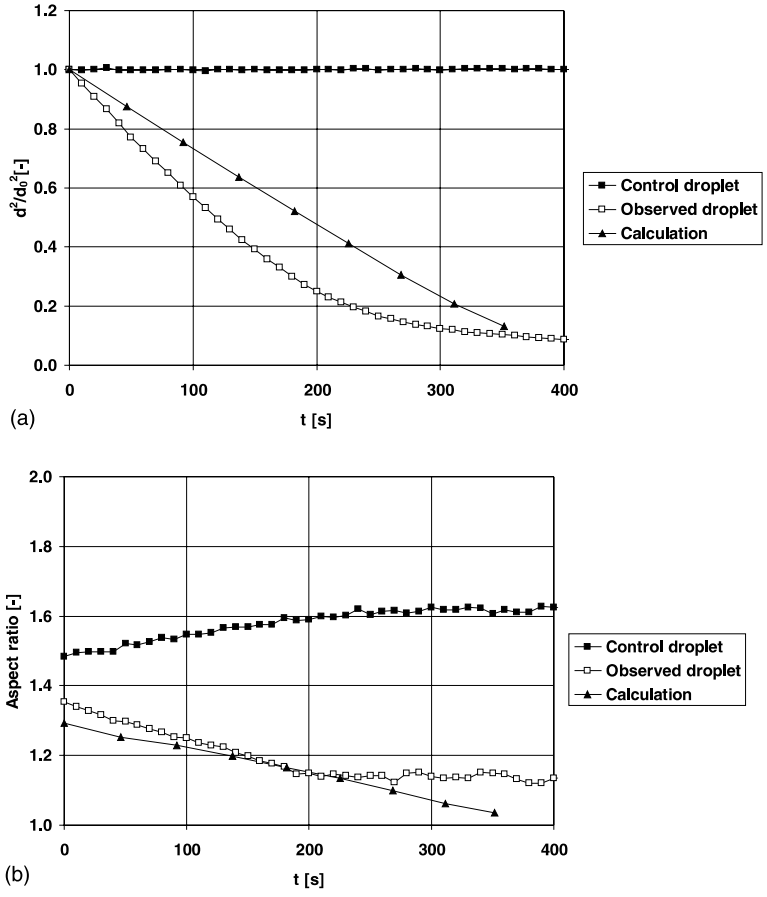

Fig. 8. Experimental and computational results for water/ethanol droplets with an initial water mass fraction of 25%: (a) normalized droplet surface and (b) aspect ratios of control and observed droplets. The initial volume of the droplets was 2.69 μl.

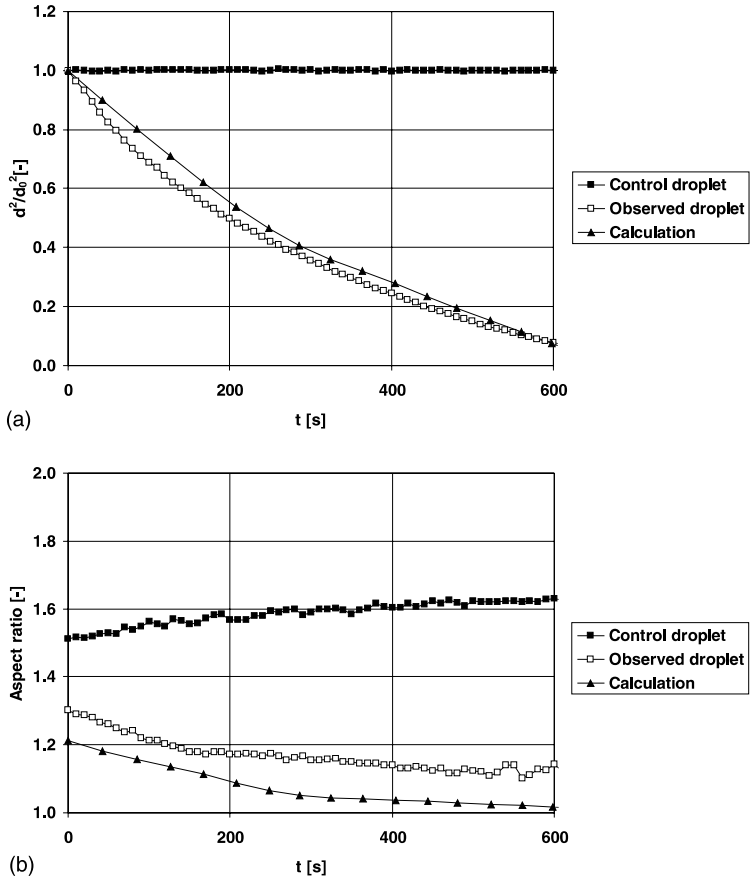

Fig. 9. Experimental and computational results for water/ethanol droplets with an initial water mass fraction of 50%: (a) normalized droplet surface, (b) aspect ratios of control and observed droplets. The initial volume of the droplets was 2.51 μl.

fraction less than 25% (Figs. 5a and 8a). The deviations for the 25%/75% water/ethanol mixture are significantly larger than those for the corresponding water/methanol mixture, which can result from the fact that the approximation of the surface tension by Eq. (50) is much less accurate for the former than for the latter (cf. Fig. 1).

The temporal derivative of the normalized droplet surface as a function of time yields useful information about the evaporation of the mixture droplets. The negative initial value of the first derivative in time is lowest for a low initial mass concentration of water for all mixtures. It increases with increasing initial water mass fraction, showing clearly the influence of water on the evaporation (water evaporates slower than both methanol and ethanol). With progressing time, the negative values of the derivative increase, indicating that the more volatile component is evaporating and therefore is depleted from the droplet. At the last stage of evaporation the derivative is nearly constant, assuming a value around -7.3×10^{-4} s^{-1}. Comparing this result with measurements for pure water in Yarin et al. (1999) it turns out that this stage represents pure water evaporation, indicating that the droplet contains no more solute at this late time.

8. Conclusions

The evaporation of acoustically levitated droplets of binary liquid mixtures was investigated theoretically and experimentally. For the theoretical description of the mass transfer, the diffusion equation inside the droplet is solved. Experiments on the evaporation of single droplets levitated in an ultrasonic levitator are carried out. Liquid mixtures consist of water and methanol or water and ethanol. Results consist of the temporal evolutions of the drop surface and the aspect ratio of the drop contour. The temporal derivative of the drop surface, which is a measure for the mass flow rate from the droplet surface, is also discussed. Comparison of the theoretical and experimental results exhibits particularly good agreement for the water/methanol droplets with high initial water mass fractions ($\geqslant 50\%$). The poorer agreement for the water/ethanol mixtures may be due to the less accurate calculation of liquid properties, like surface tension. The binary mixture droplet evaporation exhibits two stages of the evaporation, the first one dominated by the more volatile liquid.

The approach of the present work can definitely be applied to some other mixtures (e.g. fuel mixtures of

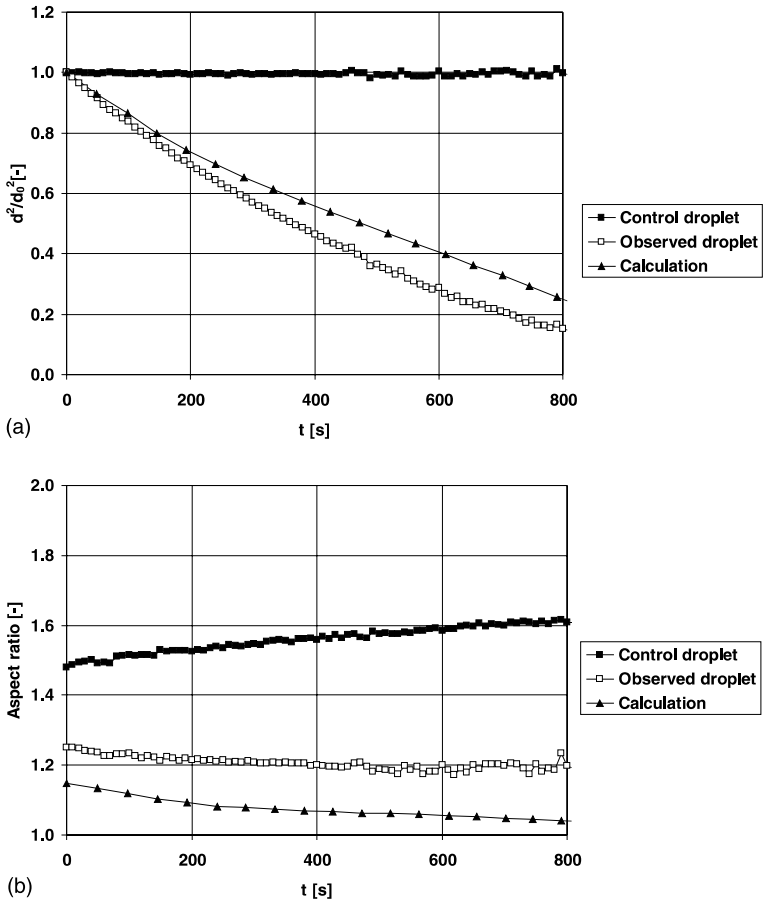

Fig. 10. Experimental and computational results for water/ethanol droplets with an initial water mass fraction of 75%: (a) normalized droplet surface and (b) aspect ratios of control and observed droplets. The initial volume of the droplets was 3.76 μl.

interest for engines), as well as to multicomponent droplets of miscible liquids. The main limitation is, however, the fact that detailed information on the activity coefficients is unavailable at present for most of the mixtures. Results on the evaporation rate in acoustic levitators shed light on the evaporation rate of droplets subject to a relatively strong forced convection, as it was shown in Yarin et al. (1999). For such a "projection", the acoustic streaming velocity should be identified with the convective flow component around the droplet in the ordinary case.

Acknowledgements

Financial support of the present work from the GIF—German–Israeli Foundation for Scientific Research and Development under grant no. I-536-097.14/97 is gratefully acknowledged. ALY was partially supported by the Fund for the Promotion of Research at the Technion. Financial support from the European Union under grant ENK6-CT-2000-00101 is gratefully acknowledged. We acknowledge gratefully the cooperation of Prof. C. Tropea at the Technical University of Darmstadt.

References

Annamalai, K., Ryan, W., Chandra, S., 1993. Evaporation of multicomponent drop arrays. Trans. ASME. J. Heat Transfer 115, 707–716.

Chen, G., Aggarwal, S.K., Jackson, T.A., Switzer, G.L., 1997. Experimental study of pure and multicomponent fuel droplet evaporation in a heated air flow. Atomiz. Sprays 7, 317–337.

Daidzic, N., 1995. Nichtlineare Tropfenschwingungen und -verdampfung in einem Ultraschall-Positionierer. PhD thesis, Lehrstuhl für Strömungsmechanik, Friedrich-Alexander-Universität Erlangen-Nürnberg.

Hirata, M., Ohe, S., Nagahama, K., 1975. Computer Aided Book of Vapor–Liquid Equilibria. Elsevier, Amsterdam.

Kays, W.M., 1975. Convective Heat and Mass Transfer, second ed. McGraw-Hill, New York.

Klotz, I.M., Rosenberg, R.M., 1994. Chemical Thermodynamics, fifth edition. J. Wiley & Sons, New York.

Law, C.K., Binark, M., 1979. Fuel spray vaporization in humid environment. Int. J. Heat Mass Transfer 22, 1009–1020.

Law, C.K., Xiong, T.Y., Wang, C.H., 1987. Alcohol droplet vaporization in humid air. Int. J. Heat Mass Transfer 30, 1435–1443.

Renksizbulut, M., Bussmann, M., 1993. Multicomponent droplet evaporation at intermediate Reynolds numbers. Int. J. Heat Mass Transfer 36, 2827–2835.

Schlichting, H., 1979. Boundary Layer Theory. McGraw-Hill, New York.

Wohlfarth, Ch., Wohlfarth, B., 1997. In: Lechner, M.D. (Ed.), Surface Tension of Pure Liquids and Binary Liquid Mixtures. Springer, New York.

Yarin, A.L., Brenn, G., Kastner, O., Rensink, D., Tropea, C., 1999. Evaporation of acoustically levitated droplets. J. Fluid Mech. 399, 151–204.

Yarin, A.L., Pfaffenlehner, M., Tropea, C., 1998. On the acoustic levitation of droplets. J. Fluid Mech. 356, 65–91.